Geophys. J. Int. (2006) **167,** 592–604 doi: 10.1111/j.1365-246X.2006.03114.x

Estimating baking temperatures in a Roman pottery kiln by rock magnetic properties: implications of thermochemical alteration on archaeointensity determinations

Simo Spassov and Jozef Hus

Section du Magnétisme Environnemental, Centre de Physique du Globe de l'Institut Royal Météorologique de Belgique, B-5670 *Dourbes (Viroinval), Belgium. E-mail: simo.spassov@oma.be*

Accepted 2006 June 11. Received 2006 June 9; in original form 2005 November 15

SUMMARY

Absolute past geomagnetic field intensity determinations requiring laboratory heating are labourious and the success rate is rather low, mostly because of induced thermochemical magnetic mineral alterations. Archaeomagnetic intensity determinations are mainly limited to displaced ceramics produced in kilns. In this study, the suitability of an *in situ* baked structure is investigated. Different magnetic properties of baked material taken from the combustion chamber wall and floor of a Roman pottery kiln, with variable colouring, are examined in dependence on the distance to the combustion chamber. The temperature distribution is reconstructed based on rock magnetic experiments after stepwise heating. The rock magnetic temperature estimates agree fairly well with a mathematical heat conduction model demonstrating the penetration of heat into the combustion chamber wall. The rock magnetic results show that blackish- and greyish-coloured kiln parts, that had been in close contact with the fuel, during ancient kiln operation, are not suitable for intensity determinations. Although sufficiently baked, they strongly alter during laboratory heating and new remanence-carrying minerals are formed. The brownish-coloured material at a distance 65–80 mm away from the combustion chamber seems to be most suitable as its magnetic properties remain nearly unchanged during laboratory heating. Rock magnetic and modelled temperature estimates for this material consistently indicate ancient baking temperatures of about 600°C. The model demonstrates that cooling takes longer in the inner parts of the combustion chamber wall. Retarded cooling affects the blocking temperatures and hence the strength of the thermoremanent magnetization. The variability of cooling rates should be taken into account when investigating archaeointensities of specimens cut from large samples, or of samples taken from different parts of a kiln.

Key words: archaeointensity, archaeomagnetism, Belgium, heat conduction, rock magnetism, Roman pottery kiln.

1 INTRODUCTION

Baked materials collected in archaeological sites provide still the most accurate and reliable absolute geomagnetic field determinations needed for the study of past field behaviour and field modelling. Archaeomagnetic reference secular variation curves, based on dated baked materials, have been established for different areas in Europe (e.g. Bucur 1994; Batt 1997; Kovacheva *et al.* 1998; Gallet *et al.* 2002; Márton 2003; Schnepp & Lanos 2005). They have reached such a precision that archaeomagnetic dating has become feasible now (e.g. Incoronato *et al.* 2002; Hus & Geeraerts 2005). Previous archaeomagnetic dating was limited to field directional data only, but often yields multiple solutions. Intensity determinations are therefore needed additionally in order to reduce the number of dating solutions. Whereas directional data are mainly obtained on non-displaced structures baked *in situ* (kilns, fireplaces, etc.), intensity determinations are generally limited to displaced wares produced in kilns (pottery, tiles, bricks, etc.). The latter are preferred for archaeointensity determinations as they are more common, solid, are thought to have been exposed to similar baking conditions and because of the high baking degree and apparent homogeneity in general. Nevertheless, ideally the field intensity should be determined on the same baked structure material that was used for directional determinations as both refer to the same time. Compared to displaced ceramics, baked *in situ* structures are better time-constrained, firing conditions are generally better known and the structures are probably thermally stabilized due to multiple firings.

Baked materials from the floor or the walls of large fired structures had been exposed to rather variable firing conditions as the variable colouring of the pottery kiln shows in Fig. 1. Hence, the

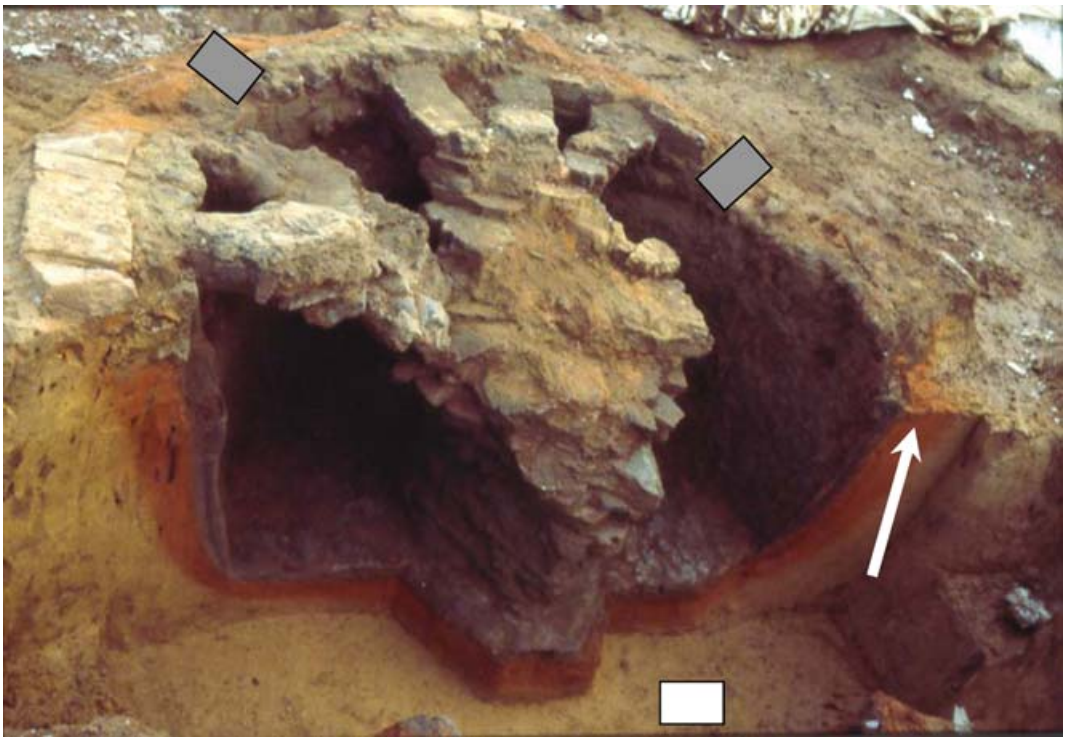

Figure 1. Roman pottery kiln BRYA03 at Bruyelle in Belgium. Almost all specimens used in this investigation originate from a 180-mm-long block sample (see Fig. 2), taken perpendicularly at the upper right-hand side of the combustion chamber wall (white arrow). The white rectangle indicates the location of the floor sample, whereas the grey rectangles indicate the approximate location of wall samples used for palaeointensity determination 107s11, 109s07 (left-hand rectangle) and 092s04, 092s07 (right-hand rectangle).

reliability of archaeomagnetic data depends strongly on the choice of appropriate samples. It has to be ensured that the material had been baked sufficiently and that post-baking neo-formation of magnetic minerals did not occur.

For absolute archaeointensity determinations, the natural remanent magnetization (NRM) is considered to be a thermoremanent magnetization (TRM) acquired during cooling in the Earth's magnetic field. The natural TRM is compared with a TRM induced in a known laboratory field of similar strength. The ratio between NRM and the acquired laboratory TRM equals the ratio between the ancient geomagnetic field and the applied laboratory magnetic field intensity. The simple method fails in the case of a multicomponent NRM, for example, due to strong viscous overprinting or when post-baking chemical alterations occurred *in situ* or during laboratory heating. In order to detect the latter, E. Thellier and O. Thellier developed the stepwise double heating method, which allows to monitor thermally induced alterations and also to increase the accuracy (*cf.* Thellier & Thellier 1959). The method was modified and different methods have been proposed later and therefore the reader is referred to Valet (2003), for a more detailed and comprehensive overview on absolute palaeointensity determinations.

The strength of a TRM depends on the blocking temperatures, which in turn depend on the cooling rate. Slower cooling rates lower the blocking temperatures and hence increase the TRM intensity as can be deduced from Néel's (1949, 1955) theory of single-domain (SD) TRM. Laboratory cooling rates are often much higher than original cooling rates, and this difference may cause erroneous archaeointensity results (Dodson & McClelland-Brown 1980; Halgedahl *et al.* 1980; Walton 1980). Genevey & Gallet (2002) observed TRM intensity overestimates between about 5 and 15 per cent for various pottery shards when cooling the samples for 33 hr instead of 0.5 hr. If the original cooling rate is known, a correction can be applied (Garcia 1996; Chauvin *et al.* 2000). However, it is obvious that the cooling rate varies in an archaeological structure, depending on the thermoconductive environment. Outer kiln parts may cool faster than inner kiln parts, resulting in different NRM intensities. This has been mentioned by Jordanova *et al.* (2003), who found large differences in firing temperature within an archaeological structure to be the major reason for variable magnetic properties of individual samples.

Magnetic mineral alteration during thermal treatment is a common problem in all methods involving laboratory heating (Jordanova *et al.* 2001, 2003). As archaeomagnetic samples had already been exposed to high temperatures during ancient times, one normally expects that laboratory heating does not affect their magnetic mineralogy considerably. There are three main causes of thermal alterations: different baking conditions, insufficient baking and post-baking weathering. Laboratory heating is generally done under oxidizing conditions. These probably did not prevail in certain kiln parts like the combustion chamber, because often wood, charcoal or coal had been used as fuel. Minerals that had been formed under reducing conditions (e.g. magnetite), become oxidized during laboratory heating and the capacity of remanence acquisition will decrease. If an archaeomagnetic sample had not been sufficiently baked and/or non-baked material appeared after baking (e.g. clay films along cracks), laboratory heating may cause neo-formation of magnetic minerals and the remanence acquisition capacity may increase. The presence of weathering products, such as iron oxihydroxides, has similar effects. Laboratory heating will transform thermally unstable minerals (e.g. goethite) into ferri- and/or antiferromagnetic phases (see Gualtieri & Venturelli 1999; Özdemir &

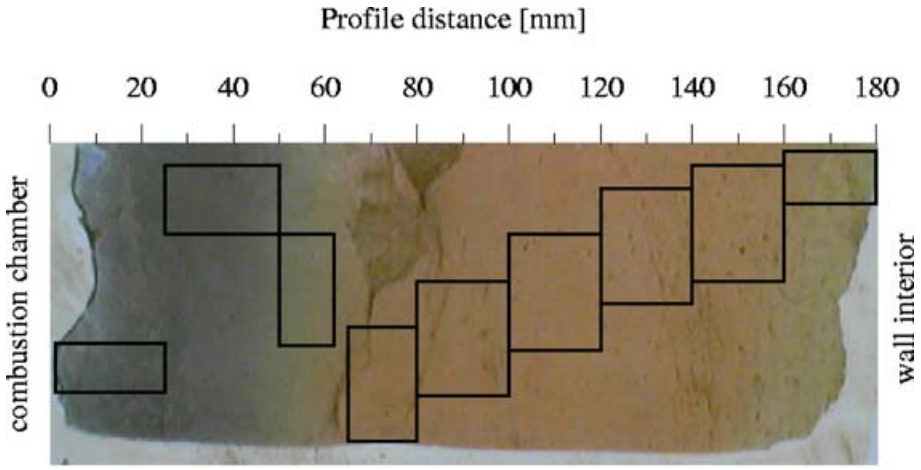

Figure 2. Block sample from the combustion chamber wall (*cf.* white arrow in Fig. 1). The different colours of the source material (loess like) indicates variable chemical environment to which the loess had been exposed during past kiln operation. Where in contact with fuel (left-hand side, 0–62 mm), reducing conditions prevailed due to higher carbon oxide concentration. Brownish colours instead, indicate rather oxidizing conditions (65 and 160 mm). Yellowish hues are visible at the utmost right-hand side of the block sample, where the loess had been less thermally influenced. Nine specimens were taken at following intervals: 0–25 mm, 25–50 mm, 50–62 mm, 65–80 mm, 80–100 mm, 100–120 mm, 120–140 mm, 140–160 mm and 140–180 mm and are indicated by the rectangles in the figure.

Dunlop 2000), which can strongly increase the remanence acquisition capacity.

This study aims at assessing the onset of magnetic mineral alteration during repeated laboratory heating by means of rock magnetic measurements, in order to determine baking temperatures and to preselect suitable material from *in situ* baked structures for archaeointensity analyses. The variability of magnetic properties of original samples from a kiln wall and floor in dependence on the distance from the combustion chamber, and their thermal stability during stepwise progressive laboratory heating will be discussed. The temperature distribution is reconstructed and modelled mathematically in order to find the most suitable parts of the baked structure for archaeointensity determinations.

2 ARCHAEOLOGICAL SITE DESCRIPTION AND SAMPLING

The samples originate from the wall and the floor of a semi-sunken Roman pottery kiln (BRYA03), unearthed at the site of the Roman villa 'Haute Eloge' in Bruyelle, Belgium (Bausier 1996). There is archaeological evidence that this Roman site had been occupied before the 2nd century AD, and coin findings suggest abandoning of the site at the end of the 3rd century (Bausier 1996). The two most probable archaeomagnetic ages for kiln BRYA03, based on archaeomagnetic directional data only, are 170 and 295 AD (Hus & Geeraerts 2005). The well-preserved pottery kiln BRYA03 is of circular shape with a central built-in pedestal and raised oven floor consisting of bar-like beams of baked clay (Fig. 1). The inner diameter of the combustion chamber is about 1.3 m at the level of the raised oven floor. The combustion chamber which shows traces of vitrification on the inner side had been dug in loess-like material.

Two samples were taken from the kiln, one from the combustion chamber wall and another in the floor. The wall sample was cut perpendicular to the wall at a spot where different colours suggest strong thermal gradients. Despite the variable colouring of the sample, no textural changes were visible and it is assumed to be homogeneous with respect to grain size and density. Fig. 1, shows a vertical transection through the combustion chamber. The white arrow in the figure indicates the location of the wall sample. Nine specimens, including less-baked loess-like material, were cut from this sample, as indicated by the rectangles in Fig. 2. The zero profile distance corresponds to the inner side of the wall facing the combustion chamber. A second sample taken 130–150 mm below the kiln floor was also studied (white rectangle in Fig. 1). Its moderate yellowish brown colour indicates that this sample had apparently not been influenced by the heat from the combustion chamber. Preliminary archaeointensities were obtained from brownish (specimens 092s07 and 109s07) and blackish/greyish (specimens 092s04 and 107s11) coloured samples taken from the combustion chamber wall (grey rectangles in Fig. 1).

The loess-like material sampled around the kiln had been contaminated by the site occupation and may had been heated partly. Therefore, also pristine Late Pleistocene loess with rock magnetic properties similar to that of the floor sample (*cf.* Table 1) was collected in a loess/palaeosol sequence at Grand Manil, about 100 km east from Bruyelle, for comparison.

Prior to rock magnetic investigations, all specimens (excluding those for archaeointensity determination) were gently crushed by hand in a mortar, in order to enlarge the specific surface of the sample and hence to better determine the onset of thermochemical magnetic mineral alteration. The crushed material was then passed through a 1-mm mesh sieve, discarding small pebbles that are occasionally present.

3 EXPERIMENTS AND PROCEDURES

Loose powder specimens were used for progressive heating experiments in the oven of a Schonstedt thermal demagnetizer. After a heating time of 0.5 hr at variable temperatures, the samples were removed from the demagnetizer and cooled in ambient air temperature to equilibrium. The following progressive heating steps were chosen: not heated, 150°C, 250°C, 350°C, 450°C, 550°C and 650°C. After each heating step, magnetic low-field susceptibility was measured in a KLY-3 Kappabridge. About three grams of powder was then pressed into small paper boxes, in order to measure acquisition curves of isothermal remanent magnetization (IRM), backfield

Table 1. Munsell colour code (Munsell 1905), magnetic low-field susceptibility, IRM at 500 mT, remanent coercive force and relative IRM loss during 100 s ($IRM/IRM_{-500\,mT,0.4\,s}$) of non-heated samples from the combustion chamber wall and the kiln floor. Pristine loess from the loess/palaeosol section Grand Manil in Belgium is given for comparison.

Specimen	Profile distance (mm)	Munsell colour code	Colour Description	χ (10^{-8} m^3 kg^{-1})	$IRM_{500\,mT}$ (mA m^2 kg^{-1})	H_{cr} (mT)	$IRM_{-500\,mT,0.4\,s}$ loss within 100 s (per cent)
Wall	000–025	0 3	Medium dark grey	329.8	329.1	79	1.5
Wall	025–050	10 YR 2/2	Dusky yellowish brown	723.8	299.6	63	6.0
Wall	050–062	10 YR 4/2	Dark yellowish brown	424.0	94.0	43	8.0
Wall	065–080	5 YR 4.5/5	Moderate/light brown	141.4	24.9	28	10.5
Wall	080–100	5 YR 4.5/5	Moderate/light brown	25.1	4.1	33	7.0
Wall	100–120	5 YR 5/6	Light brown	19.7	1.9	38	4.5
Wall	120–140	5 YR 5/6	Light brown	18.3	1.8	40	4.0
Wall	140–160	5 YR 5/6	Light brown	16.6	1.8	42	3.5
Wall	160–180	7.5 YR 5/5	Light brown/moderate yellowish brown	15.7	1.8	41	3.0
Floor	130–150	10 YR 5/4	Moderate yellowish brown	13.8	1.8	43	2.
Loess	–	11 YR 6.5/5	Greyish orange/dark yellowish orange	13.7	1.1	51	2.1

curves and short-term remanence decay after each heating step. All remanence measurements were performed in a 'rotation' magnetometer (Burov *et al.* 1986; Jasonov *et al.* 1998) in maximum magnetizing fields between +500 and −500 mT and averaged field increments of 0.5 mT per magnetization step. The magnetization duration at each magnetization step is of the order of tenths of a second. After finishing the backfield curve, the direct current was switched off and the magnetizing field decreases towards a constant rest field of about −0.4 mT within the following 0.4 s. The decay of the remaining remanence ($IRM_{-500\,mT,0.4\,s}$) was monitored during 100 s.

Filtered backfield curves were used for the calculation of remanence coercivity spectra, applying the software MAGMIX (Egli 2003).

The temperature dependence of magnetic low-field susceptibility from ambient temperature to 700°C was measured on selected specimens in a CS-3 heating unit of a KLY-3 Kappabridge in air, at a heating rate of 6°C min^{-1}.

4 RESULTS

(i) *Short-term relaxation behaviour of remanent magnetization.*

The 'rotation' magnetometer monitors the decay of the isothermal remanence ($IRM_{-500\,mT,0.4\,s}$), imparted in a field of 500 mT to the sample, for a period of 100 s. An exponential decay trend is observed in all specimens and at all heating stages (Fig. 3). The non-heated specimen that was taken very close to the fire (0–25 mm profile distance) loses very little remanence of 1.5 per cent per 100 s (Fig. 3a, Table 1). Laboratory heating has only a small influence and increases the remanence decay by only about 1 per cent. This behaviour changes for the adjacent specimen at profile distance 25–50 mm (Fig. 3b). Before laboratory heating, the remanence loss is about 6 per cent, but increases stepwise to 9 per cent after heating at 650°C. With increasing distance from the combustion chamber, the remanence loss first increases and the influence of laboratory heating decreases (Figs 3c and d). The highest remanence decay rate of about 11 per cent is observed in the specimen at 65–80 mm profile distance. The decay curves are similar for all heating degrees at this profile distance. Further away from the combustion chamber, the remanence loss decreases again and heating has almost no influence on the remanence decay, for example, sample at 160–180 mm profile distance (Fig. 3f). The specimen from below the kiln floor (130–150 mm deep) shows much larger variations during heating than the wall specimen at 160–180 mm profile distance. Before heating and at low heating temperatures, the remanence loss is about 2 per cent per 100 s, but increases at higher heating steps (Fig. 3g). Pristine loess has a decay rate similar to the specimen from below the kiln floor at low heating temperatures, but in contrast, laboratory heating hardly influences the decay rate of the former (Fig. 3h).

(ii) *Backfield curve coercivity spectra.*

Coercivity spectra were obtained by differentiation of the backfield curves. The spectra of the non-heated specimens (Fig. 4, black curves) differ considerably across the profile, indicating magnetomineralogical changes, as is also suggested by the observed change in colour (Table 1, Fig. 2). Both the IRM intensity and coercivity of remanence decrease gradually with increasing distance from the combustion chamber, from 0 to 80 mm, respectively, from 329 to 25 mA m^2 kg^{-1} and from about 79 to 28 mT (Table 1, Figs 4a–d). Progressive laboratory heating considerably decreases remanence coercivity and $IRM_{-500\,mT,0.4\,s}$ intensity (Fig. 4, Table 2). Changes occur already at 150°C (*cf.* interval 25–62 mm, Figs 4b and c).

The specimen at 65–80 mm profile distance exhibits the smallest changes in remanence intensity and coercivity over all heating steps, but the $IRM_{-500\,mT,0.4\,s}$ intensity decreases substantially after heating to 650°C (*cf.* blue and pink curves in Fig. 4d; Table 2), whereas the remanence coercivity is lowered by only a few milliTesla.

Specimens beyond 100 mm profile distance have similar coercivity spectra as shown in Fig. 4(f). The IRM intensity of the non-heated specimens decreases rapidly with increasing distance from the combustion chamber and the remanence coercivity increases again (Table 1). The coercivity spectra are not much influenced by heating up to 450°C. At higher heating degrees, a high-coercivity component starts to form (blue and pink curves in Fig. 4f), but the $IRM_{-500\,mT,0.4\,s}$ intensity remains nearly unchanged (Table 2).

The specimen from below the kiln floor exhibits spectra similar to the wall specimens far away from the combustion chamber (Fig. 4g), except that changes at lower heating temperatures are larger. The coercivity spectra of pristine loess (150°C–650°C) are similar to samples distant from the heat source (Fig. 4h). A remarkable coercivity decrease, however, is observed when pristine loess is heated from room temperature to 150°C. Such a decrease has been ascribed to stress release in low-temperature oxidized grains present in loess (Van Velzen & Zijderveld 1992; Van Velzen & Dekkers 1999). Although the IRM intensity does not change (*cf.* Tables 1 and 2), all

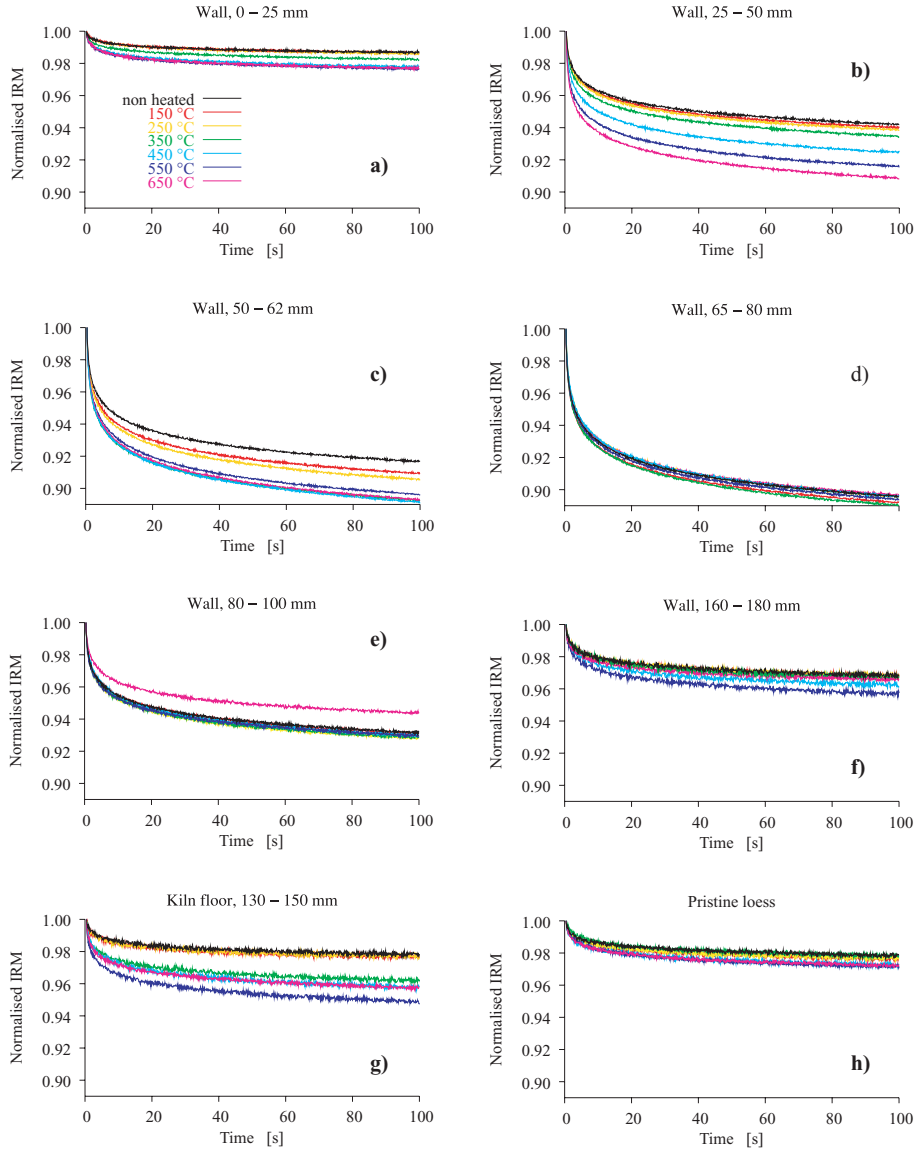

Figure 3. Short-term remanence decay of non-heated and heated specimens from the combustion chamber wall (a–f) and the kiln floor (g) at different distances from the heat source. The graphs are normalized to $IRM_{-500\,mT}$, 0.4 s after the removal of the magnetic field. The highest remanence loss is observed in the specimen at 65–80 mm profile distance (d). Laboratory heating has apparently no influence on the 10 per cent remanence loss of this specimen. A sample of pristine loess from Grand Manil (Belgium) is shown for comparison (h).

coercivity spectra are shifted to lower coercivities during heating (Fig. 4h).

(iii) *Magnetic low-field susceptibility.*

The non-heated specimen from below the kiln floor possesses the smallest susceptibility value of all kiln specimens examined (Table 1). The value of 13.8×10^{-8} m^3 kg^{-1} is similar to pristine loess from the loess section at Grand Manil, Belgium (Table 1). A small susceptibility increase is observed between 350°C and 550°C. Heating at 650°C in air reduces the susceptibility slightly, probably due to oxidation (Table 2).

The non-heated combustion chamber wall specimens between 80 and 180 mm profile distance have somewhat enhanced values as compared to the specimen below the kiln floor. With increasing distance to the combustion chamber, the susceptibility decreases slightly but consistently. Heating to 550°C does not cause substantial changes; the smallest values are observed at 650°C.

The specimens between 0 and 80 mm profile distance have considerably enhanced susceptibilities and maximum values are reached in the sample at 25–50 mm profile distance. The specimens between 0 and 62 mm are strongly affected by laboratory heating (Table 2), whereas minor changes are observed only in the specimen at 65–80 mm profile distance.

(iv) *Temperature dependence of low-field magnetic susceptibility.*

In order to obtain information on the magnetic mineralogy, the low-field magnetic susceptibility variation during heating from ambient temperature to 700°C and subsequent cooling was monitored for selected non-heated specimens (Fig. 5). The heating curve of the specimen at 0–25 mm profile distance is irreversible and characterized by a Hopkinson peak (Hopkinson 1889) that becomes more pronounced on the cooling curve (Fig. 5a). A ferrimagnetic Curie point temperature estimate of 624°C was obtained by fitting

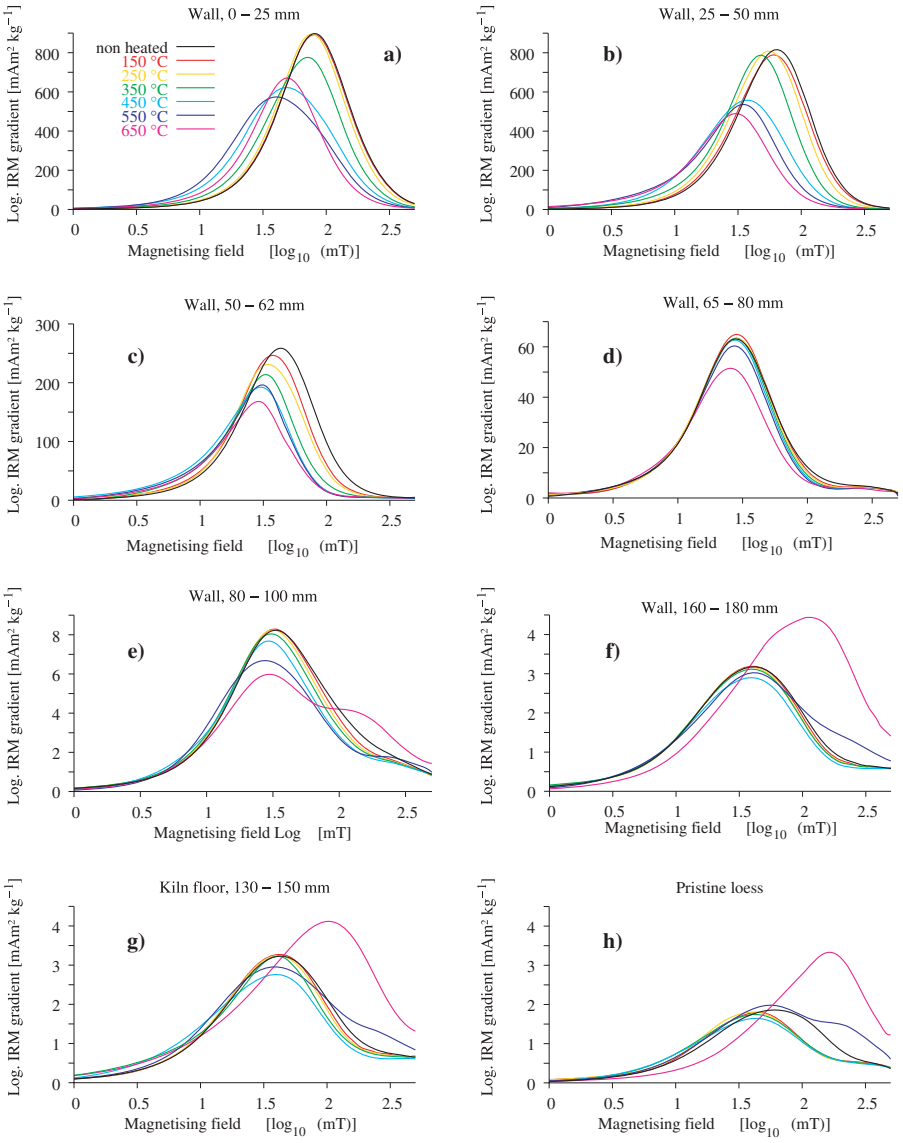

Figure 4. Coercivity spectra (logarithmic derivative of backfield curves) of non-heated and heated specimens from the combustion chamber wall (a–f) and the kiln floor (g) at different distances from the heat source. Specimens closer to the heat source are more affected by laboratory heating than specimens farther away. Minimal changes through all heating degrees occur at 65–80 mm profile distance. A sample of pristine loess from Grand Manil (Belgium) is shown for comparison (h).

Table 2. Low-field magnetic susceptibility and $IRM_{-500\,mT,0.4\,s}$ of the same samples as in Table 1 after heating at different temperatures.

Specimen	Profile distance (mm)	Low-field susceptibility (10^{-8} m^3 kg^{-1}) Heating temperature						$IRM_{-500\,mT,0.4\,s}$ (mA m^2 kg^{-1}) Heating temperature					
		150°C	250°C	350°C	450°C	550°C	650°C	150°C	250°C	350°C	450°C	550°C	650°C
Wall	000–025	340.9	365.8	421.4	527.7	595.7	549.5	329.3	326.6	300.1	282.5	270.5	245.5
Wall	025–050	796.9	882.8	989.0	1222.9	1363.8	1391.6	302.5	305.1	285.6	238.8	220.1	195.5
Wall	050–062	470.1	495.9	510.5	548.4	527.8	536.7	91.4	86.7	77.4	72.3	70.1	62.4
Wall	065–080	146.5	150.4	147.2	146.2	145.6	142.2	26.3	25.8	25.5	24.9	24.3	21.7
Wall	080–100	24.7	25.0	25.1	25.3	24.5	21.0	4.2	4.1	4.0	3.8	3.7	3.9
Wall	100–120	19.8	20.1	19.8	20.0	18.5	15.8	1.9	1.9	1.9	1.8	1.9	2.5
Wall	120–140	18.1	18.4	18.4	18.4	17.2	14.6	1.9	1.8	1.8	1.7	1.8	2.3
Wall	140–160	17.0	16.8	16.6	16.6	16.0	12.8	1.8	1.8	1.8	1.7	1.8	2.4
Wall	160–180	16.4	16.3	17.8	18.5	19.1	14.8	1.9	1.8	1.8	1.7	2.0	2.7
Floor	130–150	14.1	13.8	21.7	23.6	24.3	20.1	1.9	1.8	1.8	1.7	2.0	2.6
Loess	–	14.4	13.4	12.6	12.5	10.8	8.9	1.0	1.1	1.1	1.0	1.4	1.6

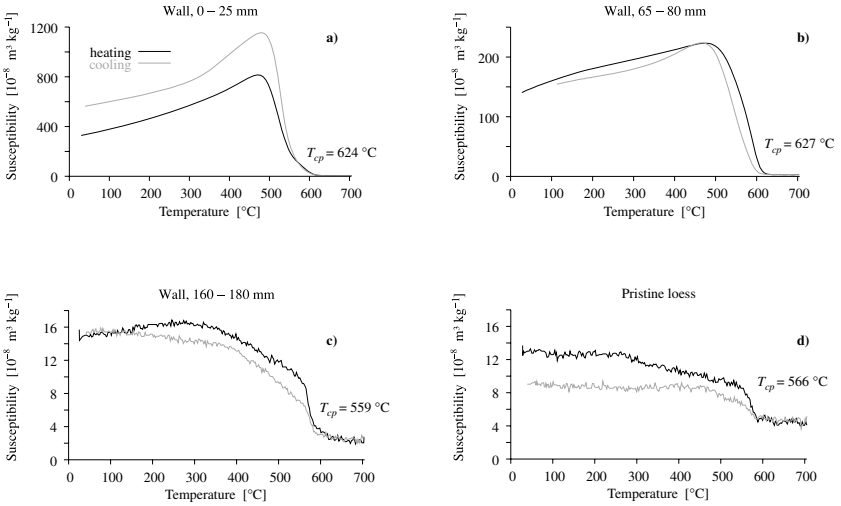

Figure 5. Temperature dependence of low-field magnetic susceptibility of three selected specimens from the kiln wall at different profile distances (a–c). Pristine loess from the Grand Manil loess/palaeosol section is shown for comparison (d). All samples have an irreversible thermal behaviour. Heating and cooling curves differ after heating to 700°C. Curie temperatures were estimated by fitting the paramagnetic part of the inverse susceptibility versus temperature relation with a hyperbolic function (Chikazumi & Charap 1964; Dunlop & Özdemir 1997).

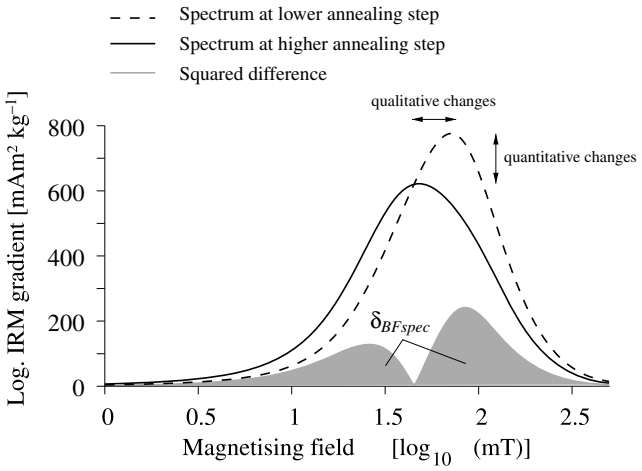

Figure 6. Quantitative assessment of thermal alteration between two consecutive heating steps, using differences in the coercivity spectrum of backfield curves. The surface below the grey shaded curve corresponds to the parameter $\delta_{BF_{spec}}$ as calculated from eq. (2). The parameter δ_{BF} allows for qualitative and quantitative changes.

the paramagnetic part of the inverse susceptibility versus temperature relation with a hyperbolic function (Chikazumi & Charap 1964; Dunlop & Özdemir 1997). Specimen 65–80 mm does not exhibit a well-defined Hopkinson peak on the heating curve, but on the cooling curve there is strong evidence for it (Fig. 5b). The Curie point temperature obtained is about 627°C. Both the wall specimen at 160–180 mm profile distance and the pristine loess sample have similar Curie point temperatures respectively of about 559°C and 566°C. A Hopkinson peak is absent on both the heating and cooling curves (Figs 5c and d). The heating curve of pristine loess is less reversible than that of the specimen at 160–180 mm profile distance. Note that fitting the paramagnetic part of the inverse susceptibility versus temperature relation with a hyperbolic function always overestimates the real Curie point (Krupička 1973).

5 INTERPRETATION AND ANCIENT BAKING TEMPERATURE ESTIMATION

(i) *Non-heated specimens.*

The short-term remanence decay (Fig. 3) can be taken as a measure for the presence of predominantly ferrimagnetic particles with relaxation times of the order of seconds. Such grains have dimensions near the threshold of the superparamagnetic (SP)/stable SD grain-size boundary or about 30 nm in the case of equidimensional haematite or magnetite grains (Dunlop & Özdemir 1997). The observed exponential decay behaviour is caused by the short acquisition time of $IRM_{-500\,mT,0.4\,s}$ which is of the order of 0.1 s. The remanence acquisition time is much shorter than the maximum relaxation time. In this case, a superposition of exponential relaxations does not result in the often observed logarithmic time dependence, but rather in an exponential time dependence (Dunlop & Özdemir 1997). The relaxation time spectrum of certain samples changes dramatically during laboratory heating.

The different colouring of the non-heated source material is caused by a variable chemical environment in the combustion chamber wall during past kiln operation. Greyish tones indicate that specimens between 0 and 62 mm had been exposed to a reducing atmosphere during firing, provided by the fuel (e.g. wood, charcoal, coal). Under such conditions, trivalent iron is reduced and magnetite formation is favoured. This is apparently proved by high susceptibility values in the greyish specimens, which are comparable to present-day industrial fly ashes from coal combustion (Heller *et al.* 1998). Enhanced susceptibility values (Table 1, specimen 25–50 mm) are partly attributed to the presence of SP grains, contributing to susceptibility but not much to remanence. The enhanced viscous remanence (Table 1, Figs 3b and c, black curves) supports this interpretation. The coercivity of remanence is rather high with respect to unbaked loess, suggesting the presence of stable SD grains. The values are comparable to the ones observed in present-day anthropogenic combustion products (Spassov *et al.* 2004). High coercive forces in SD grains can be caused by lattice substitutions. Incorporation of elements, such as aluminium, magnesium and titanium, into the magnetite crystal induces internal stress and the coercive force of substituted SD grains is then stress-controlled (Dunlop & Özdemir

1997). Day *et al.* (1977) demonstrated that stress grows with increasing titanium substitution, accompanied by coercive force and remanent coercive force increase. Specimens from 0 to 62 mm probably had been subjected to high temperatures during ancient kiln operation as traces of vitrification were observed at the inner side of the kiln. Diffusion of foreign ions, such as aluminium or magnesium, into the crystal lattice is therefore a plausible explanation for the observed high coercive forces. Low to intermediate oxidation degrees may also increase the coercive force (Dunlop & Özdemir 1997). Lattice substitutions and oxidation have opposite effects on the Curie temperature in magnetic minerals. Substitution would lower the Curie point, but oxidation instead may increase the Curie temperature as has been observed for titanomaghaemites (*cf.* Dunlop & Özdemir 1997). The estimated Curie temperature of 624°C of specimen 0–25 mm indicates an oxidized phase. Moreover, the visible tail may point to the presence of another magnetic phase (Fig. 5a).

The brownish specimen (65–80 mm) has a lower coercivity of remanence, IRM intensity and susceptibility. Susceptibility and coercivity of remanence are comparable to values for luvisols and palaeoluvisols obtained by Hanesch & Petersen (1999) and Spassov *et al.* (2003), suggesting that an oxidized low-coercivity phase, such as maghaemite, is present in this specimen (Fig. 5b). Ancient baking had apparently produced a larger amount of thermally stable short-term viscous grains compared to other specimens (*cf.* Fig. 3b).

The magnetic properties of specimens between 80 and 160 mm and from below the kiln floor are similar. The light brown colour is probably due to SP–haematite, which does not contribute much to susceptibility, because of its low saturation magnetization (Dunlop & Özdemir 1997). Specimens away from the heat source (160–180 mm in the wall; 130–150 mm in the floor) are approaching the yellowish colour of pristine loess (Table 1). The bulk magnetic properties (susceptibility, IRM intensity) are also similar to pristine loess, whereas the Curie point temperatures are different, indicating the presence of substituted magnetite in pristine loess and in specimen 160–180 mm (Figs 5c and d).

(ii) *Heated specimens.*

Laboratory heating should give evidence about the thermal stability of mineral phases in a specimen. The black to greyish specimens (0–62 mm) are expected to change their magnetic mineralogy when reheated in air, because oxidizing conditions during laboratory treatment are different from the conditions during ancient kiln operation (higher oxygen partial pressure in the thermal demagnetizer). Magnetite, if present, is expected to oxidize into maghaemite or haematite phases. The remanence coercivity is lowered strongly during heating, whereas the susceptibility increases (Figs 4a–c and 5a). The latter indicates neo-formation of predominantly ferrimagnetic phases during the measurement in the CS-3 oven. As IRM intensity decreases and susceptibility increases with increasing heating temperatures (Table 2), these newly formed magnetic phases are partly of SP nature. The susceptibility is about 1.7 times higher after heating to 550°C compared to the non-heated specimen (Table 2, specimens 0–50 mm). The susceptibility-enhancement near the Curie point is called Hopkinson peak. The enhancement factor is given by the ratio of the remanent coercive forces at room temperature (T_R) and at blocking temperature (T_B), that is, $H_{cr}(T_R)/H_{cr}(T_B)$ (Dunlop 1974). As $H_{cr}(T_R)$ decreases after heating (Fig. 4a), an increased ratio of $H_{cr}(T_R)/H_{cr}(T_B)$ would be due to an increased amount of viscous grains, lowering rather $H_{cr}(T_B)$ than $H_{cr}(T_R)$. The higher Hopkinson peak in the cooling curve in Fig. 5(a) is therefore interpreted to be caused by newly formed minerals in the vicinity of the SP/stable SD grain-size boundary. The increasing remanence loss during stepwise heating (Figs 3b and c) supports this interpretation. It remains unclear whether this newly formed SP phase results from existing SD grains or not.

The specimen at 65–80 mm profile distance shows almost no change in magnetic properties during all heating steps, except at 650°C. Apparently, the laboratory heating conditions are nearly similar to the thermal and chemical conditions during past kiln operation. The short-term viscous grain-size fraction seems, surprisingly, to be thermally stable (Fig. 3d). However, small changes are recognizable in the susceptibility versus temperature curves (Fig. 5b). After heating to 700°C, the cooling curve has a more pronounced Hopkinson peak. The smaller width of the peak in the cooling curve is due to a more narrow blocking temperature spectrum (Dunlop 1974). New viscous grains did not form during measurement; the susceptibility-enhancement is similar on the heating and cooling curves. This is in agreement with the remanence decay curves (Fig. 3d) showing no substantial neo-formation of viscous grains during laboratory heating.

At farther distances (80–180 mm), laboratory heating has little influence on magnetic parameters. New remanence carriers, but contributing little to the susceptibility, are formed above 450°C. An increased degree of non-saturation at 500 mT between 550°C and 650°C (Fig. 4e) indicates the formation of remanence-carrying haematite. From the comparison with pristine loess, it can be concluded that samples at a larger distance from the combustion chamber, between 160 and 180 mm in the wall and between 130 and 150 mm in the floor, had still been thermally influenced during past kiln operation.

The observed decrease in coercivity and increase in susceptibility in the pristine loess sample may be caused by internal stress release after heating at 150°C, which is an indicator for low-temperature oxidation (Van Velzen & Zijderveld 1992; Van Velzen & Dekkers 1999).

(iii) *Temperature estimation through rock magnetic parameters.*

The estimation of baking temperatures relies on the following concept: a sample that had been heated during past kiln operation to a certain temperature T_1 will not change its rock magnetic properties if again heated to T_1 in the laboratory under similar conditions. This holds, if the magnetic minerals had reached chemical equilibrium at T_1. When the sample is heated above T_1, magnetic minerals are not anymore in chemical equilibrium, resulting in rock magnetic property changes. This concept assumes that post-baking weathering has not occurred. The same concept is used in archaeometry, taking advantage of changes in clay mineralogy and structure during progressive laboratory heating. Maniatis *et al.* (2002), for instance, analysed after each heating step Fourier Transform Infrared Spectra (FTIS) on samples from a prehistoric burnt clay structure at the archaeological site of Archontiko (Greece) and were able to determine firing temperatures.

Rock magnetic 'palaeothermometers' have already been proposed for volcanics and weakly metamorphic sediments using progressive susceptibility versus temperature measurements (Hrouda 2003). In order to quantify any magnetomineralogical changes during laboratory heating, a general thermal alteration parameter δ (similar to the alteration parameters introduced by Hrouda *et al.* 2003) is defined as the normalized root of the squared difference of magnetic parameters between two heating steps:

$$\delta = \frac{\sqrt{(p_L - p_H)^2}}{p_L} \times 100\,\text{per cent}. \quad (1)$$

Table 3. Values of the relative thermal alteration parameter for magnetic susceptibility (δ_χ) calculated with eq. (1), and for the remanence decay curves (δ_{Jv}) and the backfield coercivity spectra ($\delta_{BF_{spec}}$) from eq. (2), for different heating steps.

Specimen and profile distance (mm)		Alteration parameter at different temperature intervals																	
		23–150°C			150–250°C			250–350°C			350–450°C			450–550°C			550–650°C		
		δ_χ	δ_{Jv}	$\delta_{BF_{spec}}$	δ_χ	δ_{Jv}	$\delta_{BF_{spec}}$	δ_χ	δ_{Jv}	$\delta_{BF_{spec}}$	δ_χ	δ_{Jv}	$\delta_{BF_{spec}}$	δ_χ	δ_{Jv}	$\delta_{BF_{spec}}$	δ_χ	δ_{Jv}	$\delta_{BF_{spec}}$
		(per cent)			(per cent)			(per cent)			(per cent)			(per cent)			(per cent)		
Wall	000–025	3	1	2	7	1	6	15	8	18	25	6	30	13	4	15	8	9	20
Wall	025–050	10	2	6	11	1	11	12	7	18	24	17	30	12	9	15	2	12	13
Wall	050–062	11	8	16	5	5	8	3	12	18	7	7	18	4	3	6	2	11	12
Wall	065–080	***4***	***1***	***4***	***3***	***2***	***3***	***2***	***2***	***3***	***1***	***2***	***3***	***0***	***3***	***4***	2	10	13
Wall	080–100	1	3	4	1	2	3	1	2	3	1	5	7	3	3	9	14	5	24
Wall	100–120	1	2	3	2	1	2	2	1	3	1	4	4	8	7	11	15	30	46
Wall	120–140	1	0	3	1	1	2	0	2	3	0	4	4	7	6	9	15	26	40
Wall	140–160	2	2	4	1	0	2	2	2	3	0	7	8	3	8	10	20	30	47
Wall	160–180	5	1	2	1	1	2	9	1	2	4	6	7	3	13	16	23	38	55
Floor	130–150	2	2	4	3	1	2	58	1	8	9	6	10	3	16	22	17	28	44
Loess	–	5	9	17	7	2	4	6	1	5	1	4	4	13	32	39	18	20	54

The parameter δ represents the relative change of a magnetic parameter p during heating from a lower temperature step (index L) to a higher temperature step (index H). In the case of susceptibility, p_L and p_H are susceptibility values at a lower and a higher heating step, respectively. Eq. (1) can be extended to curves, such as coercivity spectra:

$$\delta_{BF_{spec}} = \frac{\int_{H_{min}}^{H_{max}} \sqrt{(p_L(H) - p_H(H))^2}\, dH}{\int_{H_{min}}^{H_{max}} p_L(H)\, dH} \cdot 100\,\text{percent}, \qquad (2)$$

where $p_L(H)$ and $p_H(H)$ are the coercivity spectra at a lower and a higher heating step (H = magnetizing field) measured at room temperature. The parameter $\delta_{BF_{spec}}$ describes qualitative changes (coercivity) and quantitative changes (intensity) as seen in Fig. 6. Eq. (2) can also be applied to viscous remanence decay curves (e.g. Fig. 3). In this case, the magnetizing field H in eq. (2) has to be substituted by the time t.

Thermal alteration parameters were calculated for all samples (Table 3) and were used to assess the temperature interval to which the sample at any time during ancient kiln operation had been exposed. The samples from 0 to 62 mm profile distance cannot be used for temperature reconstructions because ancient and laboratory heating conditions are different, as previously discussed. In sample 65–80 mm, δ_χ, $\delta_{BF_{spec}}$ and δ_{Jv} change by a few per cent between all heating steps up to 550°C, but a distinct increase of about 10 per cent in $\delta_{BF_{spec}}$ and δ_{Jv} is observed during heating from 550°C to 650°C ($\delta_{Jv,\,650°C}$ and $\delta_{BF_{spec}}$, 650°C, Table 3). The parameter δ_χ, however, does not show any substantial increase. If this specimen would have been heated during kiln operation at 650°C, no magnetomineralogical changes would be expected to occur during laboratory heating up to 650°C. This is not the case from the 10 and 13 per cent increase of $\delta_{BF_{spec}}$ and δ_{Jv}, respectively. The estimated maximum ancient baking temperature of this specimen is between 550°C and 650°C. The ancient baking temperature reconstruction for the other specimens is less accurate, as the thermal alteration parameters show a rather gradual increase from step to step. Temperatures between 450°C and 550°C were estimated for the interval of 80–140 mm, 350°C and 450°C for the interval of 140–160 mm and finally 250°C and 350°C for the interval of 160–180 mm. An increase of about 10 per cent in at least one of the three thermal alteration parameters has been taken as significant change.

6 A THERMAL CONDUCTIVITY MODEL

As proposed above, the ancient baking temperature intervals at certain profile distances can be assessed by means of rock magnetic measurements in combination with stepwise laboratory heating, if the chemical environment during ancient baking and laboratory heating is similar. In the following, temporal temperature changes during kiln operation along the sampled profile (wall sample) will be simulated mathematically. Heating and cooling behaviours will be assessed using a convection-free heat-transfer model. Moving fluids, such as pore water, are assumed not to had been present in the loess-like subsurface during kiln operation. The heat transfer equation of Fourier (1822) in this case is given by

$$c\,\rho\,\frac{\partial T}{\partial t} - \nabla(\lambda\,\nabla T) = F, \qquad (3)$$

with c specific heat capacity, ρ bulk density, λ thermal conductivity, T temperature, F heat sources or sinks, t time and ∇ the Nabla-operator in Cartesian coordinates. In order to model the temperature as a function of time and profile distance, the 1-D approach of heat propagation in a long thin bar is taken, which is kept at one end at constant temperature, whereas the other end is heated and cooled. The bar should be surrounded by the same material. Heat loss through radiation can be neglected in the present case, and the right-hand side of eq. (3) becomes zero. Specific heat capacity c, bulk density ρ and thermal conductivity λ are assumed to be constant as no textural changes could be observed in the investigated sample. Density and crystallographic changes during heating may affect the thermal conductivity. In this case, the thermal diffusivity k ($k = \lambda/\rho c$) would be temperature-dependent. Baldo & dos Santos (2002) experimented with plastic refractory clay (containing 54 per cent silica), which was initially fired at 1200°C. No temperature dependence of k was observed, except for a steep increase of 14 per cent between 500°C and 600°C, attributed to silica phase transformation (α-quartz $\Leftrightarrow$ β-quartz). Yoon *et al.* (2004) simulated the temperature dependence of thermal conductivity λ for α- and β-quartz and found no substantial changes related to the phase transformation. This agrees with experimental findings from Kanamori *et al.* (1968). However, these authors observed an inversely exponential temperature dependence of λ between room temperature and 500°C. In order to simplify the model, the

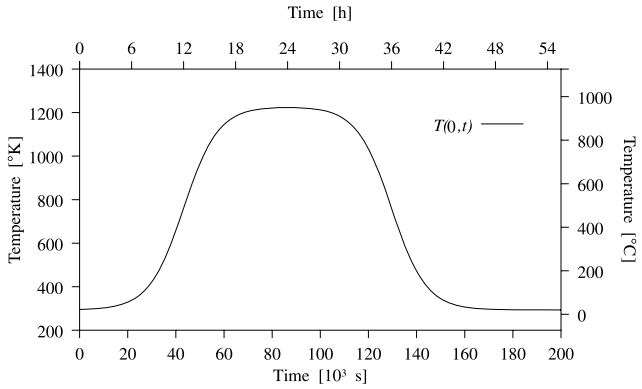

Figure 7. The boundary condition for the heat conduction model given by eq. (4) at the left-hand border ($x = 0$) is $T(0, t)$. The function describes the assumed heating and cooling processes in the combustion chamber during past kiln operation and is based on observations of a rebuilt experimental Roman kiln of similar size to that at Bruyelle (Van Heijst, private communication, 2005).

temperature dependence of the thermal diffusivity k is not considered. Under these assumptions, eq. (3) reduces to

$$\frac{\partial T}{\partial t} - k\frac{\partial^2 T}{\partial x^2} = 0, \tag{4}$$

with $k = \lambda/\rho c$ the thermal diffusivity and variable x the profile distance. Measurements of volumetric heat capacity c_v ($c_v = \rho c$) and thermal conductivity λ for dry (i.e. <0.1 volume fraction of water) silty loam or clayey loam result in thermal diffusivities of about 2.63×10^{-7} m^2 s^{-1} (Ochsner *et al.* 2001). Somewhat lower values of 1.81×10^{-7} m^2 s^{-1} were obtained by Bachmann *et al.* (2001) from investigations of air-dried soil constituents, such as subsoil silt from a Weichselian loess. Therefore, an average thermal diffusivity of 2.22×10^{-7} m^2 s^{-1} is assumed. A time dependence of the thermal diffusivity, due to changing pore water content during kiln firing, is rather unlikely.

The simulation of heating and cooling requires initial and boundary conditions, which are chosen as follows. The initial temperature at time $t = 0$ is assumed to be constant at ambient temperature, $T(x, 0) = 293$ K, at all profile distances. The temperature at the left-hand border ($x = 0$, limit of combustion chamber) is a function of time, simulating temperature rise and fall inside the combustion chamber during past kiln operation over a period of two days (Fig. 7), considered to be a typical baking time. The maximum temperature is taken as 1223 K. The assumed temperature changes are similar to observations made in an experimentally present-day rebuilt Roman pottery kiln, similar in size and shape to the one of Bruyelle (Van Heijst, private communication, 2005). The temperature at the right-hand border, which is chosen to be at 2 m ($x = 2$ m), is kept constant at ambient temperature, $T(2, t) = 293$ K.

In order to numerically solve eq. (4) with initial and boundary conditions as discussed, the problem was discretized with respect to variable x (profile distance), using second-order finite differences on a uniform grid. The resulting semi-discrete ordinary differential equations initial value problem was then integrated using the LSODA approach (Petzold 1983). All calculations were performed in Mathematica. The solution is plotted as integral surface in Fig. 8.

As expected, the temperature decreases with increasing distance from the combustion chamber. The modelled temperature at any time at the optimal profile distance 65–80 mm ranges from 580°C to 630°C, which agrees fairly well with the results from the laboratory

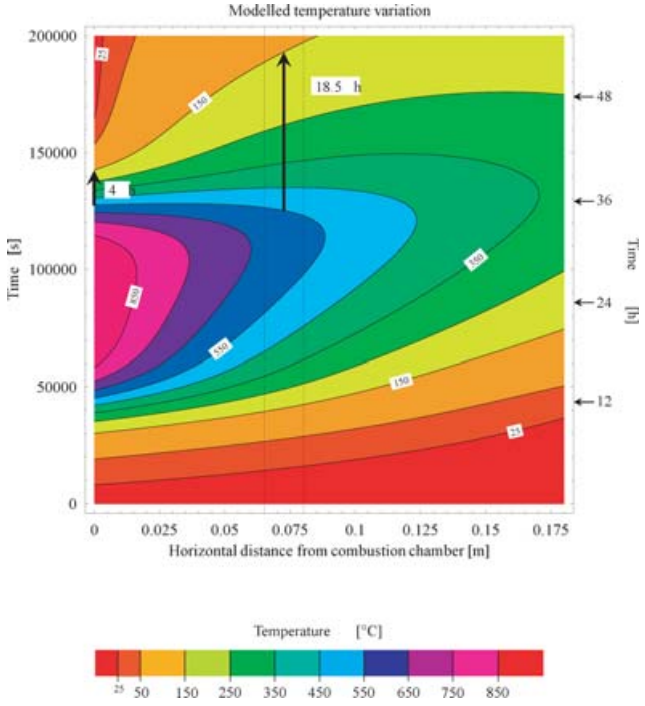

Figure 8. Solution of eq. (4) with initial and boundary conditions as discussed in the text, plotted as integral surface. The inner part of the combustion chamber wall heats up with a certain delay, for example, the maximal temperature at 0.17 m occurs about 12 hr later than in the combustion chamber. This delay causes different cooling times and rates depending on the distance from the heat source, for example, cooling in the combustion chamber from 550°C to 150°C takes 4 hr, while at the optimal profile distance of 65–80 mm (dashed vertical lines) it amounts to 18.5 hr (black arrows).

Table 4. Comparison between rock magnetic and modelled temperature estimates. The intervals of rock magnetic temperature estimates overlap with modelled temperature estimates.

Specimen	Profile distance (mm)	Rock magnetic temperature estimate (°C)	Modelled temperature estimate (°C)
Wall	000–025	–	950–800
Wall	025–050	–	800–690
Wall	050–062	–	690–640
Wall	065–080	650–550	630–580
Wall	080–100	550–450	580–540
Wall	100–120	550–450	540–470
Wall	120–140	550–450	470–420
Wall	140–160	450–350	420–370
Wall	160–180	350–250	370–330
Floor	130–150	350–250	-

heating experiments (see Table 4). The temperature at the right-hand end, at 160–180 mm profile distance, ranges from 330°C to 370°C, which is near the upper limit as suggested from the rock magnetic investigations (*cf.* Table 4). The imperfect agreement between modelled and rock magnetic temperature estimates is partly caused by the crude temperature resolution of the chosen heating steps and by limitations of the model (1-D model, temperature-independent thermal diffusivity). Moreover, the rock magnetic estimation represents only a rough temperature estimate.

Maniatis *et al.* (2002) estimated firing temperatures in ovens consisting of baked clay, using the same experimental concept as in this study. They obtained horizontal temperature gradients in the wall of a prehistoric burnt clay structure of 40–50 K cm^{-1}, which are comparable to the mean gradients of 31 and 33 K cm^{-1} respectively from our rock magnetic and modelling results (*cf.* Table 4). Schnepp *et al.* (2003) investigated the vertical heat penetration in a Mediaeval bread oven with a floor consisting of several well-separated baked loam layers. They obtained a much steeper gradient of 150 K cm^{-1} for the topmost baked loam layer. The results of Schnepp *et al.* (2003), on the contrary, are not comparable with this study. Because of low density, hot air moves aloft and hence heats up a kiln floor to a lesser extent, compared to the upper parts of a combustion chamber wall. The latter is incessantly heated by hot gases moving aloft; consequently, heat penetrates farther into the wall. The temperature gradient may therefore be higher in the kiln floor than that in the wall, if kiln floor and wall consist of the same material. This is obvious from Fig. 1, showing that the colour gradient, which qualitatively reflects the temperature gradient, varies through the kiln and is higher in the floor than that in the place where the wall sample was taken.

The model predicts that the inner parts of the combustion chamber wall heat up with delay, for example, the maximum temperature at 0.17 m occurs about 12 h later than the maximum temperature in the combustion chamber. This delay has a substantial influence on the cooling time and rate. Cooling from 550°C to 150°C takes about 4 hr in the combustion chamber, but in the wall interior at the optimal profile distance of 65–80 mm it lasts for 18.5 h, or about five times longer (black arrows in Fig. 8). The critical temperature range for the acquisition of TRM is passed through faster in the wall near the combustion chamber than farther away from it. Hence, a TRM carried by stable SD grains would be weaker near the combustion chamber than that away from it, because slower cooling through the blocking temperature interval lowers the blocking temperature and increases the TRM intensity (*cf.* Néel 1955).

7 SAMPLING STRATEGY FOR FIELD INTENSITY DETERMINATION

Chemical equilibrium of remanence-carrying minerals at elevated temperatures is the first condition to be met for successful archaeointensity determinations. The wall specimen fulfilling this requirement in the present case is found at 65–80 mm profile distance. The thermal alteration parameter δ indicates considerable changes just after heating to 550°C (Table 3). Post-baking alteration and insufficient firing are hence excluded. The remanence coercivity is about 28 mT (Table 1), which is comparable to values obtained by Jordanova *et al.* (2003) for baked clay. These authors measured somewhat lower values of 24 mT using alternating field demagnetization of isothermal remanence. This difference can be explained by the lower microcoercivity during alternating field demagnetization due to the thermal fluctuation field (Dunlop & Özdemir 1997). The backfield coercivity spectrum is rather symmetric without a significant tail towards low coercivities, as would be expected from considerable contributions of large multidomain (MD) grains. As the source material of the kiln wall is a sediment, detrital grains are certainly present and, consequently, pseudosingledomain and MD grains in specimen 65–80 mm cannot be excluded completely. At a first glance, the specimen at 65–80 mm profile length seems to be suitable for archaeointensity determinations. This specimen, however, contains the largest amount of short-term viscous grains, which are responsible for 10 per cent of the acquired IRM. As viscous samples are not suitable, one might argue that specimen 65–80 mm may not be considered for archaeointensity determinations. The performed short-term viscosity measurement spans only a time interval of 100 s after magnetization. The remanence loss within this time is comparable to the F-factor as calculated from the frequency dependence of magnetic susceptibility, rather than to the classical Thellier viscosity test (*cf.* Thellier & Thellier 1959) lasting for several weeks. Grains relaxing within the order of seconds at room temperature may not acquire a stable TRM. According to Jordanova *et al.* (2003), most archaeomagnetic samples have F-factors of about 10 per cent, being similar to our short-term viscosity index. Having these arguments in mind, specimen at 65–80 mm profile length is still considered most suitable for archaeointensity determinations.

Preliminary archaeointensity determinations have been done previously on blackish/greyish- and brownish-coloured specimens, taken at other locations in the combustion chamber wall (grey rectangles in Fig. 1). The blackish samples do not show linear segments in the Arai diagramme (Figs 9a and d); consequently, an archaeointensity determination was not possible as expected. The well-baked brownish material shows linear segments up to 400°C, giving reasonable results with small errors (Figs 9b and d). The partial TRM checks fall within the 95 per cent error envelope of the slope, indicating no substantial TRM capacity change during partial TRM acquisition. The obtained field intensities agree within the error limits with the compiled data set for western Europe given in Chauvin *et al.* (2000), after relocation to Paris.

8 CONCLUSIONS

The behaviour of rock magnetic parameters during progressive laboratory heating provides the possibility to reconstruct the temperature history of samples taken from the combustion chamber wall of a kiln. The estimates were supported by a 1-D heat conduction model, used to assess the cooling time as a function of the distance from the combustion chamber. As the baking temperatures depend on the kiln dimensions, the results obtained cannot be generalized directly to other kilns. Bearing this in mind, following conclusions can be drawn.

(1) Rock magnetic properties change considerably in the combustion chamber wall of the investigated circular Roman pottery kiln at Bruyelle (Belgium) as a function of the horizontal distance.

(2) Progressive laboratory heating in combination with rock magnetic measurements can be used to assess thermochemical alterations and to estimate the temperature distribution within the combustion chamber wall.

(3) Generally, magnetic mineral phases with different grain-size distributions coexist in baked materials. A thermal alteration parameter has been proposed which is based on magnetomineralogical changes. It is a helpful tool and should be calculated from different independent magnetic measurements in order to address the different coexisting magnetic mineral phases. The proposed parameter allows a quick test to sort out specimens which are not suitable for archaeointensity determination.

(4) At a certain profile distance in the kiln wall, the material remains almost unchanged during progressive laboratory heating up to 550°C. This optimal profile distance was estimated to occur within the interval 65–80 mm in the studied wall and represents the brownish-coloured (5YR 4.5/5 when dry) material closest to the heat source. The optimal profile distance, however, may vary inside a kiln and from kiln to kiln.

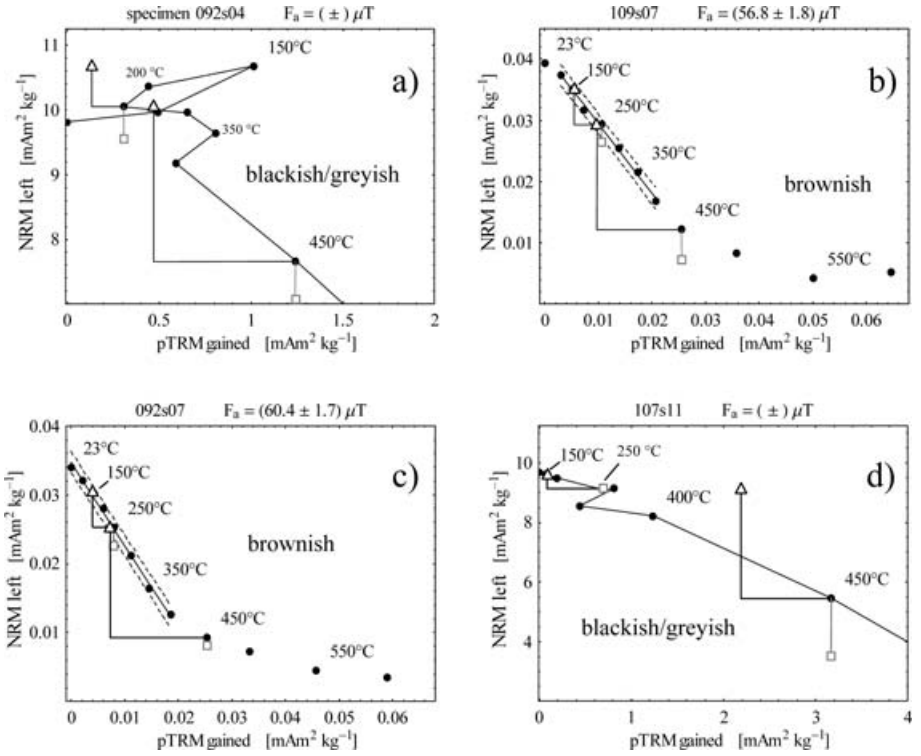

Figure 9. Arai plots of preliminary archaeointensity determinations on well-baked blackish/greyish (a, d) and brownish coloured baked clay (b, c) from Bruyelle after applying the Thellier–Thellier double heating technique (Thellier & Thellier 1959). All specimens originate from the combustion chamber wall (*cf.* Fig. 1). The blackish/greyish specimens, strongly change their TRM capacity during the procedure and show non-linear behaviour, hence yielding unreliable intensity results. The brownish specimens show linear behaviour between 100°C and 400°C. The grey squares represent residual NRM checks, that is, the residual NRM at a certain temperature should be similar after a second heating to lower temperature. The slope has been calculated for seven and eight successive temperature steps, excluding pTRM checks (black triangles), ranging from 23/100°C to 400°C for 109s07 and 092s07, respectively.

(5) Thermal gradients are well reflected by colour changes. The use of a Munsell soil colour chart during archaeointensity sampling is therefore recommended.

(6) Because of reducing conditions, greyish and blackish baked materials should be avoided for archaeointensity determinations; magnetic mineral alteration during laboratory heating is very likely to occur. Moderate to light brown (5YR 4.5/5, dry) baked material close to, but not in contact with, the heat source is in thermochemical equilibrium at elevated temperatures and seems to be more promising.

(7) The cooling rate is not constant across a large archaeomagnetic sample. During cooling, the blocking temperature interval is passed faster close to the heat source than further away. Slow cooling blocks the magnetization more efficiently at lower temperatures. The TRM acquired in SD grains is therefore stronger in samples at intermediate distances from the heat source. Hence, the cooling rate variability in baked structures must be taken into account for archaeointensity determination.

ACKNOWLEDGMENTS

The authors would like to thank Kiki van Heijst, Rob Loeffen and Frank Boot from the Bureau Archeologie Nijmegen (The Netherlands) for information concerning kiln heating. The authors also thank Diana Jordanova for having provided preliminary archaeointensity data from Bruyelle. Special thanks go to Ramon Egli for allocating his software package MAGMIX. This manuscript has benefitted a lot from constructive comments and discussions with Friedrich Heller and Ladislaus Rybach, as well as from the careful and encouraging reviews by Elisabeth Schnepp and Eduard Petrovský for which the authors are deeply grateful. This research was financed through the European research training network Archaeomagnetic Applications for the Rescue of Cultural Heritage (AARCH), contract number HPRN-CT-2002–00219 which is greatly acknowledged.

REFERENCES

Bachmann, J., Horton, R., Ren, T. & van der Ploeg, R.R., 2001. Comparison of the thermal properties of four wettable and four water-repellant soils, *Soil Science Society of America Journal,* 65, 1675–1679.

Baldo, J.B. & dos Santos, W.N., 2002. Phase transitions and their effects on the thermal diffusivity behaviour of some SiO_2 polymorphs, *Cerâmica,* 48, 172–177.

Batt, C.M., 1997. The British archaeomagnetic calibration curve: an objective treatment, *Archaeometry,* 39, 153–168.

Bausier, K., 1996. La villa romaine de la 'Haute Eloge', in *Sur la voie de l'Histoire Archéologie et TGV. Etudes et documents Fouilles 2.* pp. 67–73, ed. Matthys, A., Ministere de la Région Wallone, Direction générale de l' Aménagement du Territoire, du Logement et du Patrimoine, 168p.

Bucur, I., 1994. The direction of the terrestrial magnetic field in France, during the last 21 centuries. Recent progress, *Phys. Earth planet. Inter.,* 87, 95–109.

Burov, B.V., Nourgaliev, D.K. & Jasonov, P.G., 1986. *Palaeomagnetic Analysis*, Kazan, Kazan University Press, [in Russian].

Chauvin, A., Garcia, Y., Lanos, P. & Laubenheimer, F., 2000. Paleointensity of the geomagnetic field recovered on Archaeomagnetic sites from France, *Phys. Earth planet. Inter.,* 120, 111–136.

Chikazumi, S. & Charap, S.H., 1964. *Physics of Magnetism*, pp. 1–554, John Wiley & Sons, Inc., New York.

Day, R., Fuller, M.D. & Schmidt, V.A., 1977. Hysteresis properties of titanomagnetites: Grain size and composition dependence, *Phys. Earth planet. Inter.,* 13,260–267.

Dodson, M. & McClelland-Brown, E., 1980. Magnetic blocking temperatures of single domain grains during slow cooling, *J. geophys. Res.,* 85, 2625–2637.

Dunlop, D.J., 1974. Thermal enhancement of magnetic susceptibility, *J. Geophys.,* 40,439–451.

Dunlop, J.D. & Özdemir, Ö., 1997. *Rock Magnetism, Fundamentals and Frontiers*, pp. 1–573, Cambridge University Press, Cambridge, New York, Melbourne.

Egli, R., 2003. Analysis of the field dependence of remanent magnetization curves, *J. geophys. Res.,* 108(B2), 2081, doi 10.1029/2002JB002023.

Fourier, J., 1822. *The Analytical Theory of Heat*, pp. 1–496, republication by Dover Publications, New York (2003).

Gallet, Y., Genevey, A. & Le Goff, M., 2002. Three millennia of directional variation of the Earth's magnetic field in western Europe as revealed by archeological artefacts, *Phys. Earth planet. Inter.,* 131, 81–89.

Garcia, Y., 1996. Variation de l'intensité du champ magnétique en France durant les deux derniers millénaires, *PhD thesis*, University of Rennes, Rennes, France.

Genevey, A. & Gallet, Y., 2002. Intensity of the geomagnetic field in western Europe over the past 2000 years: New data from ancient French pottery, *J. geophys. Res.,* 107(B1), 2285, doi 10.1029/2001JB000701.

Gualtieri, A.F. & Venturelli, P., 1999. In situ study of the goethite-hematite phase transformation by real time synchrotron powder diffraction, *American Mineralogist,* 84,895–904.

Halgedahl, S., Day, R. & Fuller, M., 1980. The effect of the cooling rate on the intensity of weak field TRM in single domain magnetite, *J. geophys. Res.,* 85,3690–3698.

Hanesch, M. & Petersen, N., 1999. Magnetic properties of a recent parabrown-earth from Southern Germany, *Earth planet. Sci. Lett.,* 169, 85–97.

Heller, F., Strzyszcz, Z. & Magiera, T., 1998. Magnetic record of industrial pollution in forest soils of Upper Silesia, Poland, *J. geophys. Res.,* 103, 17 767–17 774.

Hopkinson, J., 1889. Magnetic and other physical properties of iron at high temperatures, *Phil. Trans. R. Soc. Lond., A.,* 180,443.

Hrouda, F., 2003. Indices for numerical characterization of the alteration process of magnetic minerals taking place during investigation of temperature variation of magnetic susceptibility, *Studia Geophysica et Geodaetica,* 47, 847–861.

Hrouda, F., Müller, P. & Hanák, J., 2003. Repeated progressive heating in susceptibility vs. temperature investigation: a new palaeotemperature indicator?, *Physics and Chemistry of the Earth,* 28,653–657.

Hus, J. & Geeraerts, R., 2005. Origin of deviations between the remanent magnetisation and inducing geomagnetic field directions in kilns and implications on archaeomagnetic dating, *Studia Geophysica et Geodaetica,* 49,233–253.

Incoronato, A., Angelino, A., Romano, R., Ferrante, A., Sauna, R., Vanacore G. & Vecchione, C., 2002. Retrieving geomagnetic secular variations from lava flows: evidence from Mounts Arso, Etna and Vesuvius (southern Italy), *Geophys. J. Int.,* 149,724–730.

Jasonov, P.G., Nourgaliev, D.K., Burov, B.V. & Heller, F., 1998. A modernized coercivity spectrometer, *Geologica Carpathica,* 49, 224–225.

Jordanova, N., Jordanova, D., Petrovský, E. & Kovacheva, M., 2001. Changes in magnetic properties of baked archaeological samples. *Implications for palaeointensity determination, Studia Geophysica et Geodaetica,* 45, 297–318.

Jordanova, N., Kovacheva, M., Hedley, I. & Kostadinova, M., 2003. On the suitability of baked clay for archaeomagnetic studies as deduced from detailed rock-magnetic studies, *Geophys. J. Int.,* 153,146–158.

Kanamori, H., Fujii, N. & Mizutani, H., 1968. Thermal diffusivity measurement of rock-forming minerals from 300° to 1100°K, *J. geophys. Res.,* 73,595–605.

Kovacheva, M., Jordanova, N. & Karlukovski, V., 1998. Geomagnetic field variations as determined from Bulgarian archaeomagnetic data, Part II: the last 8000 years, *Surv. Geophys.,* 19,431–460.

Krupička, S., 1973. *Physik der Ferrite und der verwandten magnetischen Oxide*. pp. 1–780, Academia, Praha.

Maniatis, Y., Facorellis, Y., Pillalim, A. & Papanthimou-Papaefthimiou, A., 2002. Firing temperature determinations of low fired clay structures, *Modern trends in Scientific Studies on Ancient Ceramics, British Archaeological Reports (International Series),* 1011,58–68.

Márton, P., 2003. Recent achievements in archaeomagnetism in Hungary, *Geophys. J. Int.,* 153,675–690.

Munsell, A.H., 1905. *A Color Notation*, Munsell Color Company, Boston.

Néel, L., 1949. Théorie du traınage magnétique des ferromagnétiques en grains fins avec applications aux terres cuites, *Annales de Géophysique,* 5,99–136.

Néel, L., 1955. Some theoretical aspects of rock magnetism, *Advances in Physics,* 4,191–243.

Ochsner, T.E., Horton, R. & Ren, T.S., 2001. A new perspective on soil thermal properties, *Soil Science Society of America Journal,* 65,1641–1647.

Özdemir, Ö. & Dunlop, D.J., 2000. Intermediate magnetite formation during dehydration of goethite, *Earth planet. Sci. Lett.,* 177,59–67.

Petzold, L.R., 1983. Automatic selection of methods for solving stiff and non stiff systems of ordinary differential equations, *Society for Industrial and Applied Mathematics Journal on Scientific and Statistical Computing,* 4, 136–148.

Schnepp, E. & Lanos, P., 2005. Archaeomagnetic secular variation in Germany during the past 2500 years, *Geophys. J. Int.,* 163,479–490.

Schnepp, E., Pucher, R., Goedicke, C., Manzano, A., Müller, U. & Lanos, P., 2003. Palaeomagnetic directions and thermoluminescence dating from a bread oven-floor sequences in Lübeck (Germany): A record of 450 years of geomagnetic secular variation, *J. geophys. Res.,* 108, doi:10.1029/2002JB001975.

Spassov, S., Heller, F., Kretzschmar, R., Evans, M.E., Yue, L.P. & Nourgaliev D.K., 2003. Detrital and pedogenic magnetic mineral phases in the loess/palaeosol sequence at Lingtai (Central Chinese Loess Plateau), *Phys. Earth planet. Inter.,* 140,255–275.

Spassov, S., Egli, R., Heller, F., Nourgaliev, D.K. & Hannam, J.A., 2004. Discrimination of atmospheric particulate matter sources with magnetic methods, *Geophys. J. Int.,* 159,555–564.

Thellier, E. & Thellier, O., 1959. Sur l'intensité du champ magnétique terrestre dans le passé historique et géologique, *Annales de Géophysique,* 15,285–376.

Valet, P., 2003. Time variations in geomagnetic intensity, *Rev. Geophys.,* 41, doi:10.1029/2001RG000104.

Van Velzen, A.J. & Dekkers, M.J., 1999. Low-temperature oxidation of magnetite in loess-palaeosol sequences: A correction of rock magnetic parameters, *Studia Geophysica et Geodaetica,* 43,357–375.

Van Velzen, A.J. & Zijderveld, J.D.A., 1992. A method to study alterations of magnetic minerals during thermal demagnetization applied to a fine-grained marine marl (Trubi Formation, Sicily), *Geophys. J. Int.,* 110,79–90.

Walton, D., 1980. Time-temperature relations in the magnetization of assemblies of single domain grains, *Nature,* 286,245–247.

Yoon, Y.G., Car, R. & Srolovitz, D.J., 2004. Thermal conductivity of crystalline quartz from classical simulations, *Physical Review B,* 70, doi:10.1103/PhysRevB.70.012302.